Highly integrated photonic crystal bandedge lasers monolithically grown on Si substrates

YAORAN HUANG[1], MINGCHU TANG[2], TAOJIE ZHOU[1], GUOHONG XIANG[1], HAOCHUAN LI[1], MICKAEL MARTIN[3], THIERRY BARON[3], SIMING CHEN[2], HUIYUN LIU[2], ZHAOYU ZHANG[1,*]

[1]*School of Science and Engineering and Shenzhen Key Lab of Semiconductor Lasers, The Chinese University of Hong Kong, Shenzhen, Guangdong, 518172, China*
[2]*Department of Electronic and Electrical Engineering, University College London, Torrington Place, London, WC1E 7JE, UK*
[3]*Univ. Grenoble Alpes, CNRS, CEA-LETI, MINATEC, LTM, F-38054, Grenoble, France*
**Corresponding author: zhangzy@cuhk.edu.cn*

Abstract: Monolithic integration of III-V lasers with small footprint, good coherence and low power consumption based on CMOS-compatible Si substrate has been known as an efficient route towards high-density optical interconnects in the photonic integrated circuits. However, the material dissimilarities between Si and III-V materials limit the performance of monolithic microlasers. Here, under the pumping condition of continuous-wave 632.8nm He-Ne gas laser at room-temperature, we achieved InAs/GaAs quantum dot photonic crystal band-edge laser, which is directly grown on on-axis Si (001) substrate, which provides a feasible route towards a low-cost and large-scale integration method for light sources on the Si platform.

1. Introduction

Advanced microscale silicon photonics technology has emerged as a promising candidate for the next-generation chip-scale data communication network due to its unique advantages of low cost, high integration density, high speed and energy efficient [1-2]. However, a highly efficient microscale Si-based light source is still considered as the obstacle for realizing a practical Si-based photonic integrated circuit (PIC), due to the indirect bandgap nature of bulk Si and Ge materials.Various approaches towards integration of microcavity lasers on Silicon substrates have been demonstrated extensively, including co-packing, hybrid integration, wafer bonding, etc. But these methods more or less include cumbersome fabrication process [1-2]. Monolithic integration method, however, is another promising route towards low cost and scalable Si-based PICs. Because monolithic integration takes advantages of advanced fabrication process of contemporary integrated circuits, in other words, it is unnecessary to consider heterogenous way to make precise alignment between light souce and other optical components. Nevertheless, the fundamental challenge of epitaxial III-V on Si is the degraded material quality caused by large material dissimilarities [3]. The planar defect, anti-phase boundary, due to the polar on non-polar growth, can be avoided by employing pretreated double-atomic-step Si substrate [4]. Furthermore, strained-layer superlattice (SLS) has been used as defect filter layers to significantly reduce the threading density defect caused by the lattice mismatched heteroepitaxial growth of III-V materials on Si [5]. Those works pave the demonstration of high-performance ridge-waveguide lasers with quantum dot (QD) gain medium directly grown on the group-IV substrates through various intermediate buffer layers and offcut substrates, including Ge [6], Ge-on-Si [7], GaP/Si(001) [8], patterned on-axis Si(001) [9]and Si substrate with 4º offcut angle [3]. However, the relatively large footprint of ridge-waveguide laser limits the realization of microscale Si-based PICs. Recently, we have demonstrated InAs/GaAs QD microdisk lasers and photonic crystal L3 defect membrane lasers monolithically grown on CMOS-compatible on-axis Si (001) substrates [10-11].

Meanwhile, defect-free photonic crystal bandedge lasers arrays enable a large-area coherent oscillation, so a large number of attractive applications have been derived [12-13], including laser-based processing and light detection. The group velocity in energy band diagram is derived by differentiating the relative dispersion. When a mode with group velocity close to zero within the material gain region, the bandedge effect occurs, which means there is a large increase in optical path length for bandedge point and significantly improve the effective gain. Various high performance photonic crystal bandedge surface emitting lasers has been demonstrated with high output power and single mode emission [14-15].

In this paper, we demonstrate InAs/GaAs QD square lattice

photonic crystal bandedge lasers monolithically grown on on-axis Si (001) substrate with ultra-low lasing threshold under 632.8nm He-Ne gas laser source at room temperature. This square-lattice photonic crystal bandedge laser on Si can be a promising candidate for the coherent light source for Si photonics due to its low threshold characteristic and potential capability for high power output.

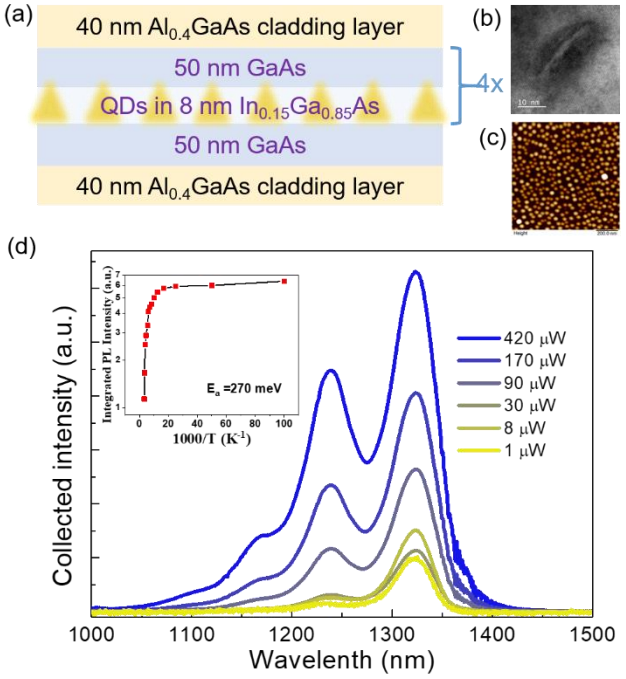

Fig. 1. (a) Schematic epitaxial structure of the active region with total thickness ~ 362 nm (b) A high-resolution STEM image of a single InAs QD. (c) An AFM image of uncapped InAs/GaAs QDs. (d) Collected PL spectra of the as-grown structure under various input optical powers at room temperature. Inset: Temperature dependent integrated PL intensity.

2. Device Fabrication

The doping-free CMOS-compatible on-axis Si (001) substrates are offered for the monolithic growth of InAs/GaAs QD photonic crystal bandedge lasers [11]. As grown 400 nm GaAs layer is on the on-axis Si (001) substrate with a 0.15 ° misorientation with two steps by metalorganic chemical vapor deposition, then the substrate is transferred to the MBE chamber for the subsequent material growth. Four sets of optimized defect filter layers (DFLs) are grown after a 200 nm of GaAs buffer layer which is grown at 580 ℃ to make the epitaxial surface smooth, while each set of DFL contains a low-temperature grown of $In_{0.18}Ga_{0.82}As$/GaAs SLSs at 450 ℃, followed by an in-situ thermal annealing at 600 ℃ for 5 mins and then a 300nm GaAs spacer layer is covered at the top with high temperature. Fig. 1(a) shows the specific details of the epitaxial structure of the active layer, four-stack as grown InAs/InGaAs dot-in-well (DWELL) active layers used as the gain materials were grown on a 1 μm $Al_{0.6}Ga_{0.4}As$ sacrificial layer [16], which were sandwiched by two symmetrical 40 nm $Al_{0.4}Ga_{0.6}As$ cladding layers. Each stack of DWELL layer consists of 2.7 Monolayer (ML) InAs QDs grown at 510 ℃ on a 2 nm $In_{0.15}Ga_{0.85}As$ layer and capped by a 6 nm $In_{0.15}Ga_{0.85}As$ layer, followed by a 5 nm low-temperature grown GaAs layer and 45 nm high-temperature grown GaAs spacer layer at 600 ℃. Fig. 1(b) illustrates a high-resolution transmission electron microscope (TEM) image of a single QD, with a typical size of 25 nm in diameter. Fig. 1(c) presents uncapped InAs/GaAs QDs grown on Si (001) substrate which is captured by atomic force microscope (AFM), with a density of about 4×10^{10} cm^{-2}. The optical property of as-grown QDs is

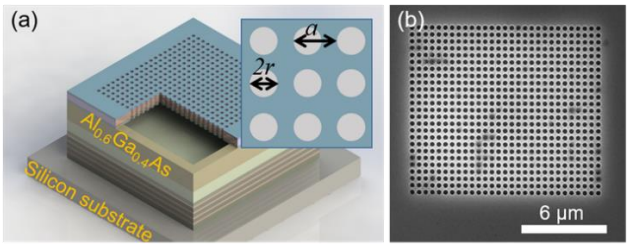

Fig. 2. (a) A schematic diagram of the fabricated InAs/GaAs QD bandedge laser directly grown on on-axis Si (001) substrate. The lattice constant and radius of air holes are a and r, respectively. (b) A SEM image of fabricated photonic crystal bandedge cavity.

investigated by a micro-photoluminescent (μ-PL) measurement under room temperature, as presented in Fig. 1(d), showing various PL spectra under different continuous-wave optically pumping powers from 1μW to 420 μW. A ground state emission of 1322 nm is observed, accompanying with a 1st excited state of 1240 nm. PL emission from the further excited states of QDs are pumped out while increasing the powers. Furthermore, am integrated PL intensity driven from temperature dependent PL measurement is presented in the inset of Fig. 1 (d), showing a thermal activation energy of approximately 270 meV, which is fitted by the Arrhenius equation.

Fig. 2(a) shows the schematic figure of the photonic crystal bandedge lasers monolithic grown on on-axis Si (001) substrate, the lattice constant a and the air holes diameter 2r are pointed in the inset. The suspension structure is formed by wet etching the sacrificial layer underneath active layer due to the different etching selection ratio. The purpose of suspension structure is to better confine the light in vertical direction, where the active layer is sandwiched by air with relative large different refractive index.

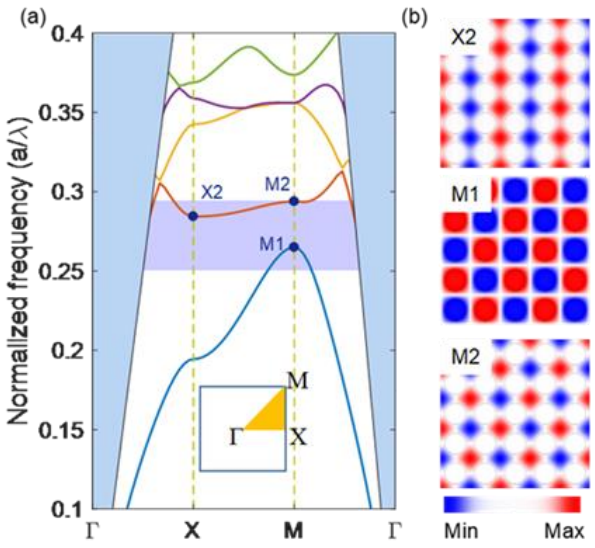

Fig. 3. (a) The dispersion relation diagram of TE-like states for the photonic crystal bandedge cavity with the parameters of r/a = 0.35 and the slab thickness 1.05a. The inset shows the irreducible Brillouin zone. The shaded blue region indicates the light cone and the purple area represents the gain region of as-grown QDs. High symmetry points with low group velocity within the gain region are marked as X2, M1 and M2. (b) The corresponding calculated Hz field profiles.

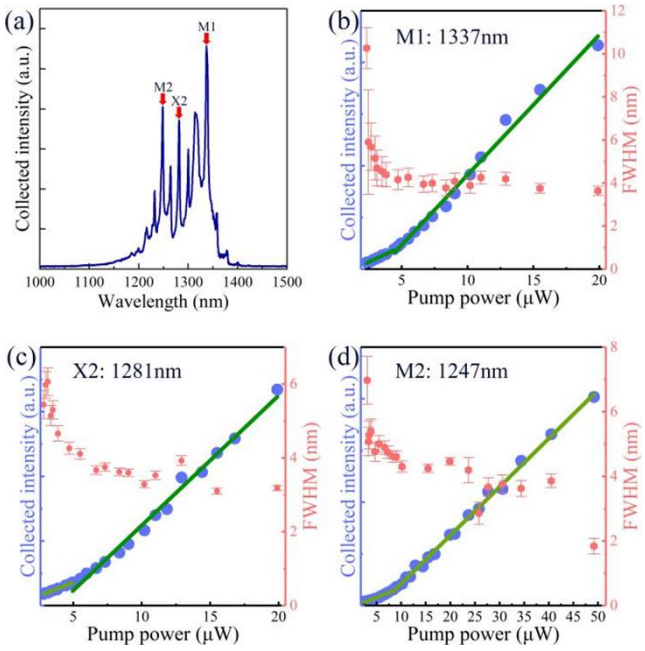

Fig. 4. (a) Emission spectrum of the fabricated photonic crystal bandedge laser, the pump power is 49.2μW. Lasing modes of M1, X2 and M2 can be determined by the spectral positions. (b)(c)(d) The L-L curve and FWHM as a function of input power for three lasing modes M1, X2, M2, respectively.

The fabrication processes of this bandedge laser are presented with these steps. First, plasma-enhanced chemical vapor deposition (PECVD) was used for depositing ~ 120nm SiO_2 as hard mask. Then ~ 160nm Zep520 E-beam resist was spin-coating on the surface of this wafer, the pattern of photonic crystal bandedge cavities array was defined by using electron-beam lithography (EBL) and followed by development. Hard mask is etched by inductively coupled plasma reactive ion etching (ICP) to transfer the pattern. After the removal of the remaining resist, ICP is using for further transformation of square lattice photonic crystal array to active region. The wet-etching process was implemented to remove the hard mask and to undercut the sacrificial layer for the formation of a free-standing photonic crystal structure. The fabricated photonic crystal bandedge cavity is shown in Fig. 2(b), which is captured by scanning electron microscope (SEM).

3. Discussion

The dispersion relation diagram and the corresponding eigen-field profiles were calculated by MIT photonic bands based on the plane-wave expansion method [17]. The dispersion relation diagram of TE-like states is illustrated in Fig. 3(a), with the bandedge cavity parameters of lattice constant a=340nm, r/a=0.35 and the slab thickness ~ 1.05a. The light cone is indicated by the blue region. The approximate optical gain region (from 1194 nm to 1340 nm) of the as-grown QDs was represented by the purple region, covering both the ground state and the first excited state obtained by curve fitting of the collected PL spectra. Three bandedge modes at high symmetry points M1, X2, and M2 are possible for the lasing emission because of their locations in the gain region. The corresponding magnetic field profiles of X2, M1 and M2 are depicted in Fig. 3(b). For further research, to realize single mode emission, so methods can be figured out by slightly changing the dielectric energy band and air energy band of dispersion relation diagram. For example, parameters of photonic crystal bandedge cavity can be optimized to ensure only one bandedge point lying within as-grown InAs QDs gain region to meet the requirement of single mode lasing. Introducing taper region (with linear decrease of air holes) at Γ point to reduce radiation loss at X2 can also be a convincing way.

A μ–PL system setup was used to characterize the fabricated photonic crystal bandedge lasers. We optically pumped our bandedge cavity at room temperature with a standard 632.8 nm He-Ne gas laser as pumping source, whose standard Gaussian spot size is around 3 μm. The PL spectrum of this cavity with a = 340nm and r/a = 0.35 was shown in Fig. 4(a). M2, X2 and M1 low group velocity points are shown in Fig. 4(a), and the spectral positions of lasing modes are comparable with the calculated normalized frequencies. The light-out light-in (L-L) curves of the three modes are showed in Fig. 4(b)-(d), with a linewidth narrowing observed. But, it is worth mentioning that due to some imperfection fabrication results, the full width at half maximum (FWHM) ~3nm of lasing modes are relatively large. The optimization of etching can make the surface of photonic crystal bandedge cavity smoother, the sidewall of the air hole more vertical, and the diameter of the air hole close to the simulation result, so as to solve the problem of large FWHM. The bandedge modes M1 and X2 emission peaking at 1337 nm and 1281 nm are within the ground state with a lasing threshold around 4 μW and 5 μW,

respectively, while the bandedge mode M2 with a peak wavelength 1247 nm was in the first excited state, of which the threshold is ~ 7.5 μW.

4. Conclusion

In conclusion, we have demonstrated InAs/GaAs QD square-lattice photonic crystal bandedge lasers monolithically grown on on-axis Si (001) substrates. The lasers operated under continuous-wave optical pumping at room-temperature. Ultra-low lasing threshold was observed in a multi-mode lasing operation. With further structure design or optimized plasma etching profiles, a single mode lasing emission is feasible. The demonstrated photonic crystal bandedge lasers monolithically grown on Si substrate are a promising candidate as a large-scale coherent light source for the Si photonics.

Funding

This research was supported by National Science Foundation of China under Grant No. 62174144, Shenzhen Fundamental Research Fund under Grant No. JCYJ20210324115605016 and N0. JCYJ20210324120204011, the Optical Communication Core Chip Research Platform, Shenzhen Key Laboratory Project under Grant No. ZDSYS201603311644527, Longgang Key Laboratory Project under Grant No. ZSYS2017003 and No. LGKCZSYS2018000015, Longgang Matching Support Fund No. CXPTPT-2017-YJ-002 and No. 201617486 and President's Fund (PF01000154), UK Engineering and Physical Sciences Research Council (EP/P006973/1 and National Epitaxy Facility), European project H2020-ICT- PICTURE (780930) and Royal Academy of Engineering (RF201617/16/28), French government managed by ANR under the Investissements davenir ANR-10-IRT-05 and ANR-15-IDEX-02 and French RENATECH network.

Acknowledgement

The devices were manufactured in Core Research Facilities (CRF) at SUSTech, and the authors would like to thank the engineers for their technical support.

Reference

1. D. Thomson, A. Zilkie, J. E. Bowers, T. Komljenovic, G. T. Reed, L. Vivien, D. Marris-Morini, E. Cassan, L. Virot, J.-M. Fédéli, J.-M. Hartmann, J. H. Schmid, D.-X. Xu, F. Boeuf, P. O'Brien, G. Z. Mashanovich and M. Nedeljkovic, "Roadmap on silicon photonics," Journal of Optics 18, 073003 (2016).
2. M. Asghari and A. V. Krishnamoorthy, "Energy-efficient communication," Nature Photonics 5, 268 (2011).
3. S. Chen, W. Li, J. Wu, Q. Jiang, M. Tang, S. Shutts, S. N. Elliott, A. Sobiesierski, A. J. Seeds, I. Ross, P. M. Smowton and H. Liu, "Electrically pumped continuous-wave III-V quantum dot lasers on silicon," Nature Photonics 10, 307 (2016).
4. R. Alcotte, M. Martin, J. Moeyaert, R. Cipro, S. David, F. Bassani, F. Ducroquet, Y. Bogumilowicz, E. Sanchez, Z. Ye, X. Y. Bao, J. B. Pin, and T. Baron, "Epitaxial growth of antiphase boundary free GaAs layer on 300mm Si (001) substrate by metalorganic chemical vapour deposition with high mobility," APL Materials 4, 046101 (2016).
5. M. Tang, S. Chen, J. Wu, Q. Jiang, K. Kennedy, P. Jurczak, M. Liao, R. Beanland, A. Seeds and H. Liu, "Optimizations of defect filter layers for 1.3-μm InAs/GaAs quantum-dot lasers monolithically grown on Si substrates," IEEE Journal of Selected Topics in Quantum Electronics 22, 1900207 (2016).
6. H. Liu, T. Wang, Q. Jiang, R. Hogg, F. Tutu, F. Pozzi, and A. Seeds, "Long-wavelength InAs/GaAs quantum-dot laser diode monolithically grown on Ge substrate," Nature Photonics 5, 416 (2011).
7. A. Lee, Q, Jiang, M. Tang, A. Seeds and H. Liu, "Continuous-wave InAs/GaAs quantum-dot laser diodes monolithically grown on Si substrate with low threshold current densities," Optics Express 20, 22181 (2012).
8. D. Jung, J. Norman, M. Kennedy, C. Shang, B. Shin, Y. Wan, A. C. Gossard, and J. E. Bowers, "High efficiency low threshold current 1.3 μm InAs quantum dot lasers on on-axis (001)GaP/Si" Applied Physics Letters 111, 122107 (2017).
9. Y. Wan, Q. Li, A. Y. Liu, A. C. Gossard, J. E. Bowers, E. L. Hu, and K. M. Lau, "Optically pumped 1.3 μm room-temperature InAs quantum-dot micro-disk lasers directly grown on (001) silicon," Optics letters 41, 1664 (2016).
10. T. Zhou, M. Tang, G. Xiang, B. Xiang, S. Hark, M. Martin, M.-L. Touraton, T. Baron, Y. Lu, S. Chen, H. Liu, Z. Zhang, "Ultra-low threshold InAs/GaAs quantum dot microdisk lasers on planar on-axis Si (001) substrates," Optica 11, 1 (2020).
11. T. Zhou, M. Tang, G. Xiang, X. Fang, X. Liu, B. Xiang, S. Hark, M. Martin, T. Baron, S. Pan, J.-S. Park, Z. Liu, S. Chen, Z. Zhang, H. Liu, "Continuous-wave quantum dot photonic crystal lasers grown on on-axis Si (001)," Nature Communications 11, 1 (2020).
12. H.-Y. Ryu, S.-H. Kwon, Y.-J. Lee, Y.-H. Lee, and J.-S. Kim, "Very-low-threshold photonic band-edge lasers from free-standing triangular photonic crystal slabs," Applied physics letters 80, 3476 (2002).
13. S.-H. Kwon, H.-Y. Ryu, G.-H. Kim, Y.-H. Lee, and S.-B. Kim, "Photonic bandedge lasers in two-dimensional square-lattice photonic crystal slabs," Applied Physics Letters 83, 3870 (2003).
14. H.-Y. Lu, S.-C. Tian, C.-Z. Tong, L.-J. Wang, J.-M. Rong, C.-Y. Liu, H. Wang, S.-L. Shu, and L.-J. Wang, "Extracting more light for vertical emission: high power continuous wave operation of 1.3-μm quantum-dot photonic-crystal surface-emitting laser based on a flat band," Light: Science & Applications 8, 108 (2019).
15. S. Noda, K. Kitamura, T. Okino, D. Yasuda, and Y. Tanaka, "Photonic-crystal surface-emitting lasers: Review and introduction of modulated-photonic crystals," IEEE Journal of Selected Topics in Quantum Electronics 23, 1 (2017).
16. HY Liu, IR Sellers, TJ Badcock, DJ Mowbray, MS Skolnick, KM Groom, M Gutierrez, M Hopkinson, JS Ng, JPR David, R Beanland, "Improved performance of 1.3 μm multilayer InAs quantum-dot lasers using a high-growth-temperature GaAs spacer layer," Applied Physics Letters 85, 704 (2004)
17. S. G. Johnson and J. D. Joannopoulos, "Block-iterative frequency-domain methods for Maxwell's equations in a planewave basis," Optics Express 8, 173 (2001).

Disclosures. The authors declare no conflicts of interest.